LOW-ENERGY PARTICLE RADIATION ENVIRONMENT AT SYNCHRONOUS ALTITUDE

E. G. Shelley and S. K. Lew

Lockheed Palo Alto Research Laboratory

Low-energy charged particles in the space environment are known to be important contributors to the degradation of thermal control surfaces on satellites and may affect thin films such as cover materials used in connection with large flexible solar arrays. These particle-induced degradation effects are of particular importance in planned future satellite projects with projected lifetimes up to ten years. Early measurements in the vicinity of synchronous altitude showed that intense and highly variable fluxes of protons and electrons with energies between one and 50 keV populate this region of space. The ATS-5 satellite, launched into synchronous orbit in August 1969, was the first synchronous satellite to include instrumentation for the investigation of the plasma properties of these low-energy charged particles. The Lockheed Palo Alto Research experiment on ATS-5 measured electron and proton fluxes in the energy range from approximately one-half to several hundred keV with primary emphasis on the region below 50 keV which contains most of the plasma energy. A statistical analysis of the data, sampled over the period from September 1969 through December 1969, shows systematic variations in the average low-energy particle radiation environment at synchronous altitude with local time and magnetic activity (K_p). The existence of a systematic variation with K_p suggests the possibility of estimating the environment under various conditions of magnetic activity from the present data.

INTRODUCTION

Both laboratory simulations and in situ satellite measurements have shown that many of the commonly used low α_s/ϵ thermal control surface materials are degraded not only by solar ultraviolet radiation, but also by low-energy charged particle radiation (refs. 1-19). This is dramatically shown in figure 1 which compares the degradation rate of $Zn0$/Sil measured on several satellites. The degradation rate was significantly greater for the synchronous and deep space satellites which were exposed to much greater low-energy particle fluxes. A detailed knowledge of the charged particle environment is therefore essential to proper design of long-lived spacecraft. Prior knowledge (refs. 20 and 21) of the environment at synchronous altitude has been extremely sketchy, based primarily on measurements from satellites with highly eccentric orbits. Since these satellites are able to acquire only a few seconds of data in the region of synchronous altitude once every few days they do not provide sufficient data to define the morphology of this dynamic region.

The ATS-5 satellite, which was launched in August of 1969, was the first synchronous satellite to carry experiments capable of spectral measurements of the low-energy electrons and protons. It carried a magnetometer and several particle detectors spanning the energy range from 50 eV to 30 MeV. The Lockheed experiment was designed to perform a survey of particle fluxes of auroral energies. It consists of eleven individual detectors, each of which measures protons or electrons in a specific energy interval spanning the range from about one-half to several hundred keV. Primary emphasis was placed on the region below 50 keV which contains most of the plasma energy. Particles in this energy region have been shown to be very important in thermal control surface damage (ref. 2).

A preliminary report on the general characteristics of the particle fluxes at synchronous altitude has been given by Sharp et al. (ref. 22). It was

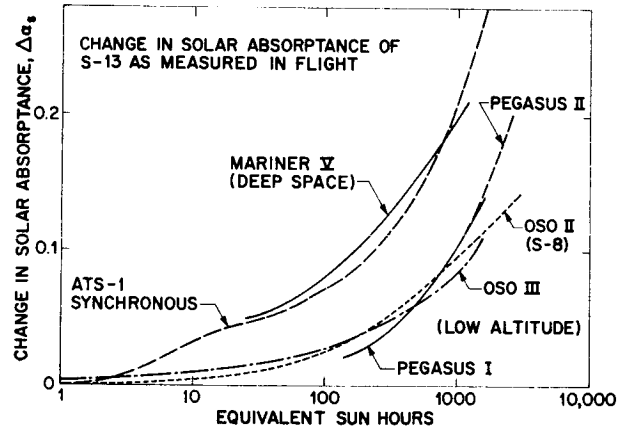

FIGURE 1.--Comparison of degradation of S-13 (ZnO/Sil) measured on several satellites. The degradation rate is significantly increased at synchronous orbit and in deep space where the particle radiation environment is enhanced (from ref. 1).

reported that large increases in the electron fluxes were observed on most nights in the vicinity of local midnight with increases of one or two orders of magnitude occurring within times ranging from a few minutes to the order of an hour and that these electron "events" were generally associated with magnetic substorms as established from auroral zone magnetograms in the vicinity of the foot of the field line passing through ATS-5. A more detailed study of the time characteristics of these electron events has also been published

(ref. 23). As reported in ref. 22, the proton fluxes were also observed to vary, but by a much smaller factor in general. A general discussion of the low-energy particle populations at synchronous orbit observed on ATS-5 has also been given by DeForest and McIlwain (ref. 24). An indication of the dramatic variations in the particle fluxes and their dependence on local time and magnetic activity is given in figures 2 and 3. Figure 2 shows the relative flux of the 6- to 18-keV electrons for two of the days included in this study. The lower and upper curves correspond to magnetically quiet and magnetically active days, respectively. During a significant part of the day the fluxes on the active day exceed those of a quiet day by about two orders of magnitude. Figure 3 shows a similar comparison for protons with energies greater than 38 keV. While the differences are not as great as those for electrons, they still differ by a factor of 5 or greater.

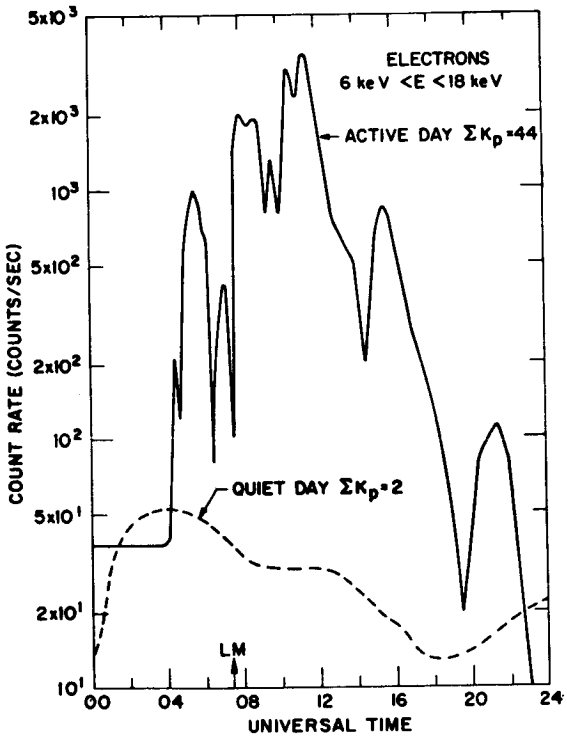

FIGURE 2.--Comparison of relative low-energy electron flux for two days of significantly different magnetic activity. Local midnight is indicated by the arrow marked LM.

In this paper, a statistical analysis of the data for 20 days spanning the period from September 1969 through December 1969 is presented. As shown in figure 4, the distribution of magnetic activity during the data samples of this study was very similar to the distribution of magnetic activity for the entire four-month period spanned by the data samples. It is therefore reasonable to treat this body of data as representative of this period. The local time dependence of four plasma parameters, electron number flux, electron average energy, proton number flux and proton average energy, was analyzed using the entire body of data. In addition, we present the results of an investigation of the dependence of these parameters on magnetic activity in several different local time sectors in the hope that this information will make it possible to extrapolate the present data to periods of differing magnetic activity.

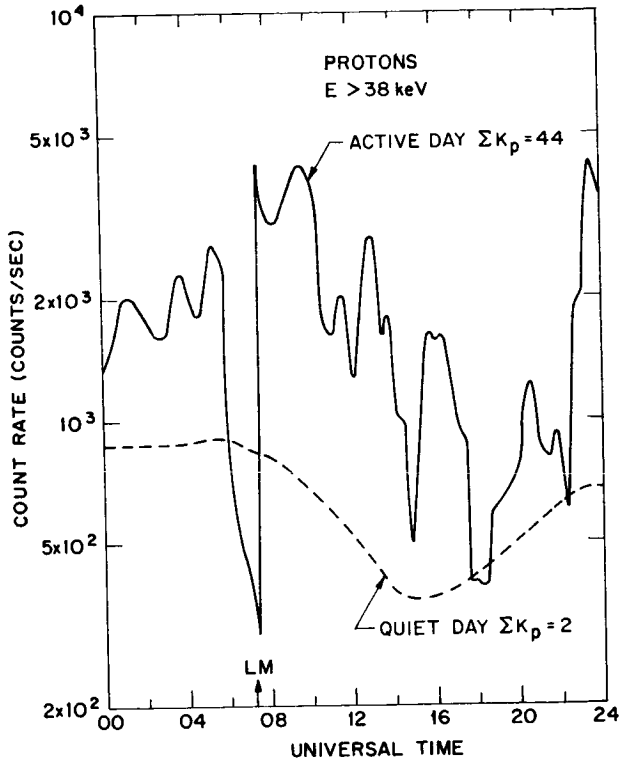

FIGURE 3.--Comparison of relative proton flux for two days of differing magnetic activity. LM indicates local midnight.

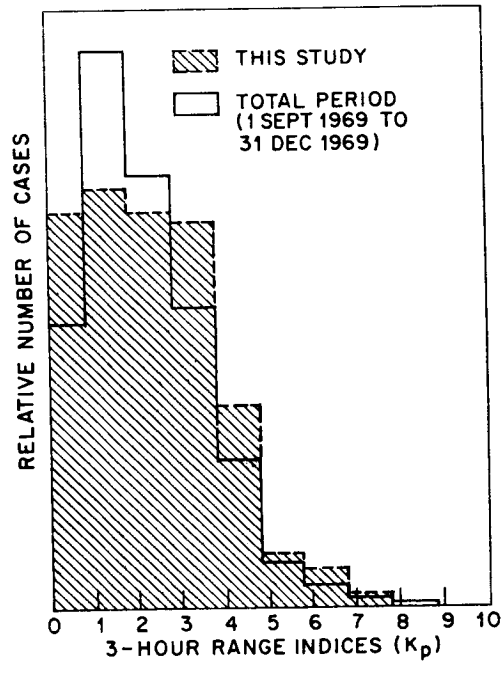

FIGURE 4.--Comparison of magnetic activity during the sample periods selected for this study with magnetic activity during the entire period from which samples were selected.

INSTRUMENTATION

The electron data presented here are from four broadband differential electron flux detectors, each consisting of a permanent magnet spectrometer which utilizes 180° deflection to achieve continuous sensitivity over a broad energy interval ($\Delta E/E \cong 100\%$). Together, the four detectors provide continuous and nearly uniform coverage for electrons over the energy range from 0.65 to 53 keV. The proton data to be presented are from three integral proton detectors with foil-determined thresholds at approximately 5, 15 and 38 keV. The minimum data sample rate for these detectors was once per telemetry sequence of 5.12 seconds. Relevant parameters for these seven detectors are given in table 1. A detailed description of the instrument and a description of the procedures used for calibration of the electron channels have been published (refs. 25 and 26).

Detector	Particle	Energy Range (keV)	Acceptance Angle (Full Angle)	Geometric Factor (cm^2-ster)
CMEA	e^-	0.65 - 1.9	$15^\circ \times 25^\circ$	1.4×10^{-5}
CMEB	e^-	1.8 - 5.4	$15^\circ \times 25^\circ$	1.0×10^{-5}
CMEC	e^-	5.9 - 17.8	$15^\circ \times 25^\circ$	1.2×10^{-5}
CMED	e^-	17.4 - 53.0	$15^\circ \times 25^\circ$	0.9×10^{-5}
CFPA	p^+	> 5	20°	3×10^{-5}
CFPB	p^+	> 15	20°	3×10^{-5}
CFPC	p^+	> 38	20°	4×10^{-4}

TABLE 1.--Detector Parameters

•For the period of the data presented here, the ATS-5 satellite was nearly stationary in geographic longitude at approximately 150°W. It was spin stabilized with spin axis approximately parallel to the earth's axis. The Lockheed experiment view direction made an angle of 11° to the spin axis, so that the detectors were sensitive to particles with pitch angles over a range of greater than 40°. This range was reduced somewhat when the spin axis was within 20° of the local magnetic field direction. The ratemeter time constants were such that the detectors averaged the flux over all pitch angles accepted. The range of pitch angles sampled varied with local time and magnetic activity, but on the average the central angle varied from about 35° near local midnight to less than 10° near local noon. It should be borne in mind that the loss cone at synchronous altitude is only about 5° full angle, so that even when the loss cone is included in the solid angle of the detectors, they are primarily sensitive to trapped particles.

DATA ANALYSIS

In order to calculate the plasma properties, such as average energy and omnidirectional-number flux, from out observations, it was necessary to make certain assumptions about the spectral and pitch-angle distributions. We assumed isotropy for both electrons and protons. This is not expected to have a large effect since, as discussed above, our detectors average over a relatively large range of pitch angles. However, because of the local time dependence of the magnetic field direction, the apparent local time dependence of the plasma parameters could be influenced by anisotropic pitch-angle distributions. That this anisotropy in our energy range is not on the average large (i.e., greater than about 2) is supported by our observations during an earlier spin mode in which the Lockheed experiment swept through all pitch angles during each spin period (ref. 22) and further by a second low-energy particle experiment on ATS-5 which had detectors at two angles (ref. 24).

The spectral model for electrons used in this analysis was as follows. The differential flux was assumed to be flat over the energy range of each of the two lower electron detectors. A function $F(E) = F_o e^{-E/E_o}$ was fit to the upper two electron channels and was used to describe the spectrum from 6 keV to 55 keV. The dependence of the calculated plasma parameters on the details of the spectral shape was tested by using other simple shapes and it was found that the results were not generally affected significantly. Similarly, the proton spectrum was assumed to be flat between the threshold energies of the lower two detectors (5 keV to 15 keV) and an exponential distribution was fit to the upper two detectors. The electron properties discussed here are for the energy range 0.65 to 55 keV and the proton properties are for energies greater than 5 keV.

With the above assumptions, the omnidirectional number fluxes (i.e., 4π times the average directional flux) and the number-density-weighted average energies for electrons and protons were calculated. Flux-weighted average energies are more appropriate for damage analysis and are generally greater than the density-weighted average energies by 10% to 50% for both electrons and protons and within the accuracy of this analysis can be assumed to be a constant 30% greater.

The plasma properties were first calculated at approximately 90-second intervals for all of the data, then averaged over one-hour periods. Each sample discussed in the following analysis and tabulated in table 2 corresponds to one of these one-hour averages.

The uncertainties in the data arising from counting statistics and other random errors are completely negligible compared with the possible systematic errors. The total systematic errors arising from all causes such as uncertainties in absolute geometric factors, spectral shapes and pitch-angle distributions were estimated at about 30% for the electron properties and 50% for the proton properties.

LT ↓ / K_p →	0^o-1^-	1^o-2^-	2^o-3^-	3^o-4^-	4^o-5^-	5^o-6^-	6^o-7^-	7^o-8^-	Total
00-03	14	8	13	12	4	4	1	0	56
03-06	15	5	15	9	4	1	3	0	52
06-09	14	11	8	15	3	2	3	0	56
09-12	11	13	10	8	9	1	2	0	54
12-15	8	13	9	13	10	2	0	1	56
15-18	8	16	12	12	4	0	0	2	54
18-21	11	18	14	10	4	0	0	0	57
21-24	11	14	11	11	9	2	0	0	58
Total	92	98	92	90	47	12	9	3	443

TABLE 2.--Number of 1-hour samples in study as a function of K_p and local time

15-6 1302-307

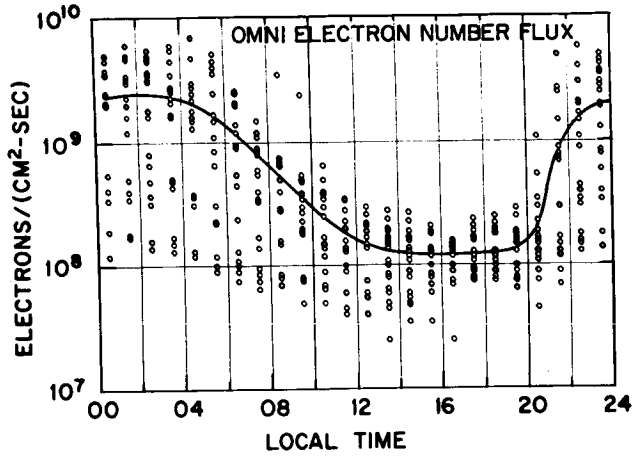

FIGURE 5.--Omnidirectional electron number flux as a function of local time. All one-hour-average samples are included. The solid curve is the average local time dependence of the flux, independent of magnetic activity.

RESULTS

Local Time Dependence

The first analysis of the data was in terms of local time dependence only, that is, there was no selection of the data on the basis of magnetic activity. In figures 5 through 8, we present the omnidirectional electron number flux, the electron average energy, the omnidirectional proton number flux, and the proton average energy, respectively. All data were included to show the variance, the solid curves give the average local time dependence. These figures are discussed separately below.

Omnidirectional Electron Number Flux (figure 5): A strong local time dependence in the overall average electron number flux is clearly evident. The average flux varies from approximately 2.5 x 10^9 electrons/cm^2-sec around midnight and early morning to 1 x 10^8 electrons/cm^2-sec near dusk. The total variation in the hourly averaged electron number flux exceeds a factor of 200; on a shorter time scale, these fluxes have been observed to vary over a range of several thousand. Another interesting observation from figure 5 is that the variation in the electron flux is much greater (~ 60X) near local midnight than around 1800 LT (~ 3X).

Average Electron Energy, Density-Weighted (figure 6): The statistical average of the electron energy has a relatively strong local time dependence. It maximizes at a value of about 13 keV near 1600 LT, approximately the time at which the electron number flux is minimum. The minimum energy, approximately 5.5 keV, occurs about 6 hours later at 2200 LT. The independent one-hour average samples of the average electron energy vary over a range from 2 keV to 22 keV. In contrast to the electron number flux, the variation in average electron energy is greatest near local dusk and smallest near local midnight.

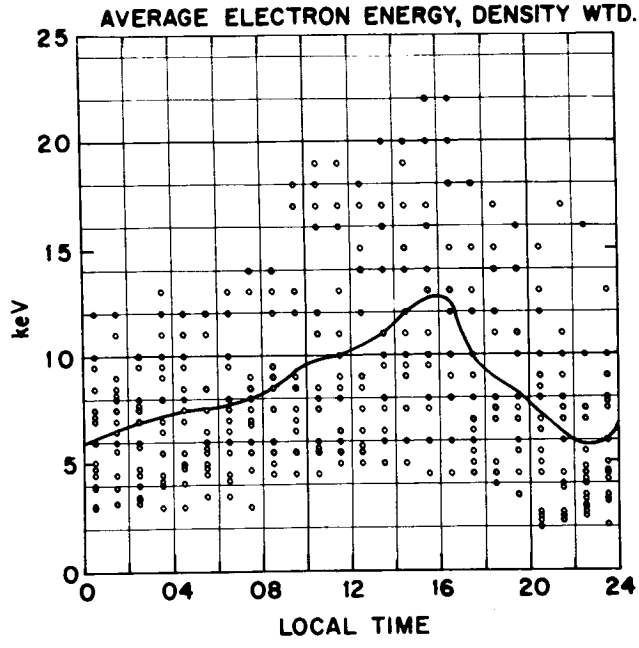

FIGURE 6.--Density-weighted average electron energy over the energy range 0.65 keV to 55 keV as a function of local time. All one-hour-average samples are included independent of magnetic activity. The solid curve is the statistical average of the electron energy as a function of local time.

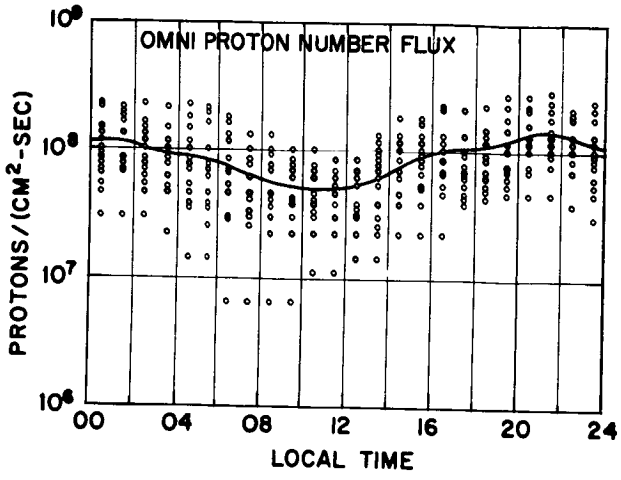

FIGURE 7.--Omnidirectional proton number flux as a function of local time for protons with energy greater than 5 keV. All one-hour-average samples are included independent of magnetic activity. The solid curve is the statistical average.

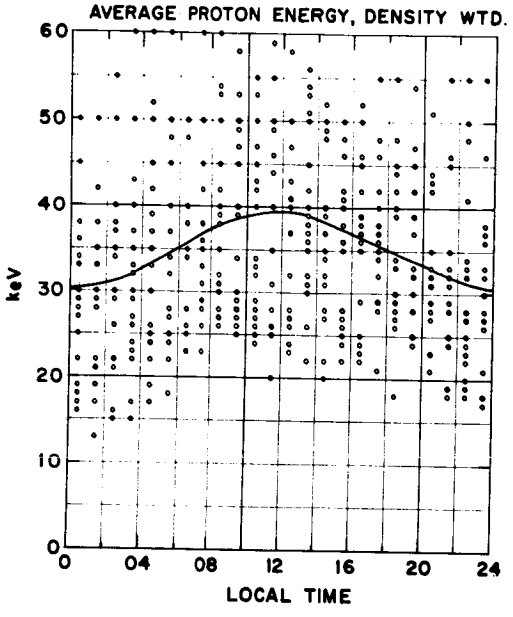

FIGURE 8.--Density-weighted average proton energy as a function of local time, $E_p > 5$ keV. All one-hour-average samples are included independent of magnetic activity. The solid curve is the statistical average dependence to the average proton energy on local time.

Omnidirectional Proton Number Flux (figure 7): The grand average proton flux is approximately 10^8 protons/cm^2-sec. In contrast to the electron flux, the apparent diurnal variation in the average proton flux is rather small (~ 3X). The local time dependence is also different, peaking about 3 hours before local midnight and reaching a minimum very near local noon. Because this variation has very nearly the same local time dependence as the systematic variation in the pitch-angle range being sampled (see the data analysis section), a significant part of this apparent diurnal variation could be explained by a pitch-angle distribution peaked at 90°. However, based on the arguments presented earlier, we estimate that at least half of this effect is a true variation in the average flux. The proton flux at a fixed local time is seen to vary by approximately a factor of 10, somewhat less than the variation observed for electron fluxes, but nevertheless highly significant.

Average Proton Energy, Density-Weighted (figure 8): The average of the proton energy is approximately out of phase in local time with the average proton flux, with the percentage variation (~ 20%) much less. The total range of the one-hour average samples is from approximately 15 keV to 60 keV with a mean of approximately 35 keV.

Magnetic Activity Dependence

An investigation of the dependence of the plasma parameters on magnetic activity was undertaken in hopes of finding relationships to make it possible to extrapolate the present data to periods of different magnetic activity. Because of the strong local time dependence of the parameters found above, the data were analyzed in 3-hour local time segments; however, where the local time effect appeared to be small these were later averaged over 6-hour segments. Table 2 shows the breakdown of the distribution of one-hour-average data samples in terms of local time and magnetic activity (K_p). This breakdown left approximately 10 samples per local time segment for each magnetic activity interval ($\Delta K_p = 1$) up to $K_p = 4$. Above $K_p = 5$, the number of samples per interval was generally 3 or less and this should be borne in mind in interpreting the results presented below.

For each of the four parameters we present a scatter plot of the parameter versus K_p for a single local time segment to demonstrate the scatter of the data. Included in these plots is a curve passing through the averages over each ΔK_p interval; the intervals are identical to those in table 2. The error bars are one standard deviation of the mean. Following each of the scatter plots is a second figure showing the average curves for each local time segment. Standard deviations are included for only a few of the points on these curves to avoid further confusion in the figures. Some "error bars" were considered necessary to indicate the significance of the fluctuations in the curves.

Omnidirectional Electron Number Flux (figures 9 and 10): The scatter in the data points within a single ΔK_p interval in figure 9 for the local time segment of zero to 0300 is typical of all of the local time segments. The average curves for all eight local time segments are included in figure 10. Several systematic effects are apparent: 1) the local time dependence is significantly less at low K_p than for high K_p; 2) the local time region from 2100 to 0600 is most sensitive to magnetic activity, but shows a saturation effect above $K_p = 3$; 3) the local time region from noon to dusk (i.e., 1200-1800 LT) is on the average unaffected by magnetic activity; and 4) the intermediate local time intervals show a slow transition in their dependence on magnetic activity from that characteristic of the midnight region to that characteristic of the afternoon region.

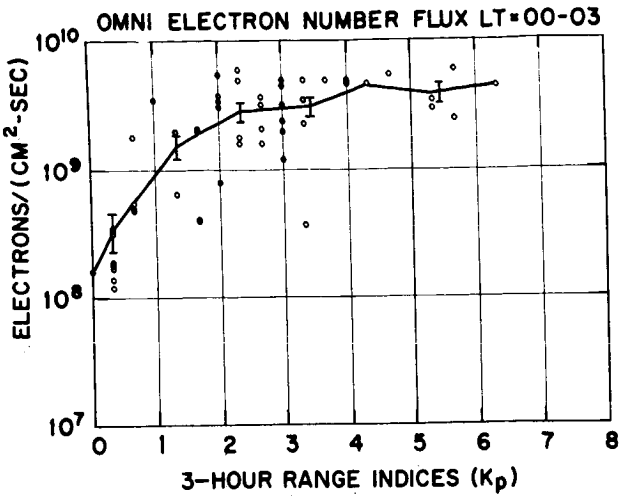

FIGURE 9.--Omnidirectional electron number flux as a function of magnetic activity (K_p) for the local time segment 0000 to 0300. The data points include all samples for this local time period. The solid curve passes through the statistical mean for each ΔK_p interval. The error bars indicate one standard deviation on the mean.

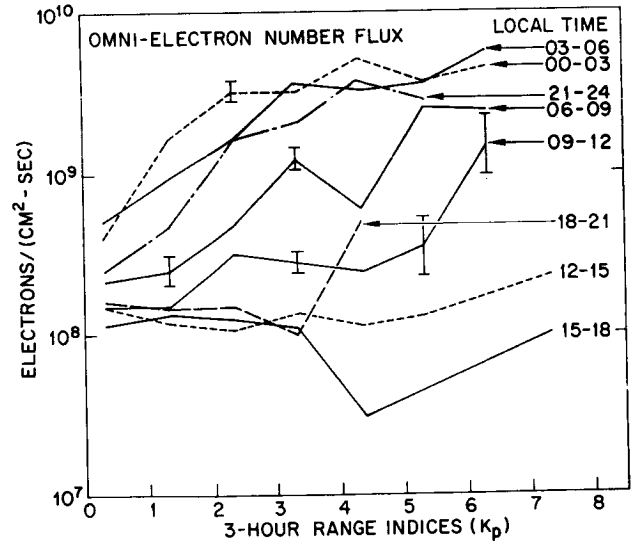

FIGURE 10.--Average dependence of the omnidirectional electron number flux on magnetic activity for each 3-hour local time segment. The error bars where given are one standard deviation on the mean.

The peaks and troughs in these curves, such as that near $K_p = 4$ on the 06-09 curve, cannot be considered statistically significant; however, the error analysis suggests that the average electron number flux can be corrected for magnetic activity within about a factor of two.

Electron Average Energy (figures 11 and 12): The scatter in the average electron data shown in figure 11 is typical for all local times except for the region 00-06 LT where the scatter is significantly less. The effect of increased magnetic activity on the average energy as a function of local time (see figure 12) is very different from the behavior observed for the electron flux. The systematic effects are as follows: 1) the local time dependence is minimal for low K_p, as was the case for the electron flux; 2) the local time region from 2100 to 0300 is least sensitive to magnetic activity; in contrast the electron flux is most sensitive in this time region; 3) in the local time region from pre-noon to dusk (0900-1800 LT) the electron energy is strongly dependent on magnetic activity up to about $K_p = 3$ or 4, followed by a saturation effect or a possible reversal (the points around $K_p = 7$ must not be given much significance since they result from only one or two samples -- see table 2). Again this contrasts with the behavior of the electron flux which was not significantly affected in this general local time region; 4) as was the case with the electron flux, the intermediate local time regions display a smooth transition in behavior between the extremes of 2) and 3) above; and 5) there is considerable evidence for a decrease in mean energy with increased magnetic activity above $K_p \simeq 5$ for most local times.

The average effect of magnetic activity on the electron average energy can be estimated from these curves with an accuracy of 20 or 30 per cent. The combined effects of magnetic activity on the electron flux and the electron average energy lead to the result that the general trend is toward increased electron energy flux with increased magnetic activity at all local times. In the vicinity of local midnight, the flux increases with little change in average energy, while in the noon to dusk region, the mean energy increases with little change in number flux. Both parameters increase in the intermediate local time regions.

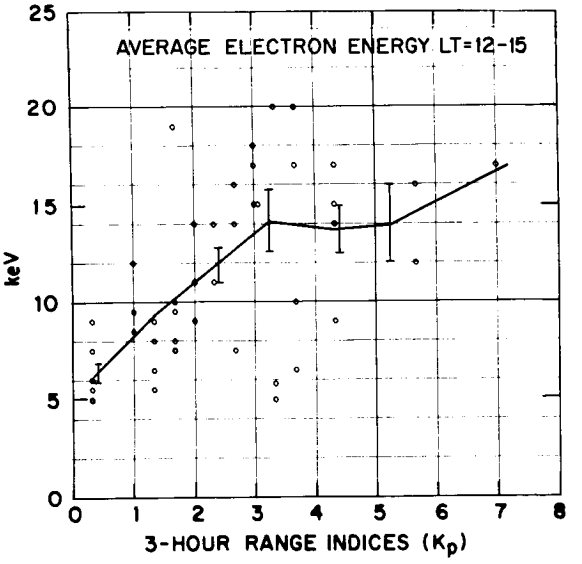

FIGURE 11.--Average electron energy as a function of magnetic activity (K_p) for the local time segment 1200 to 1500. The data points include all one-hour-average samples for this local time segment. The solid curve passes through the mean for each ΔK_p interval. The error bars are one standard deviation on the mean.

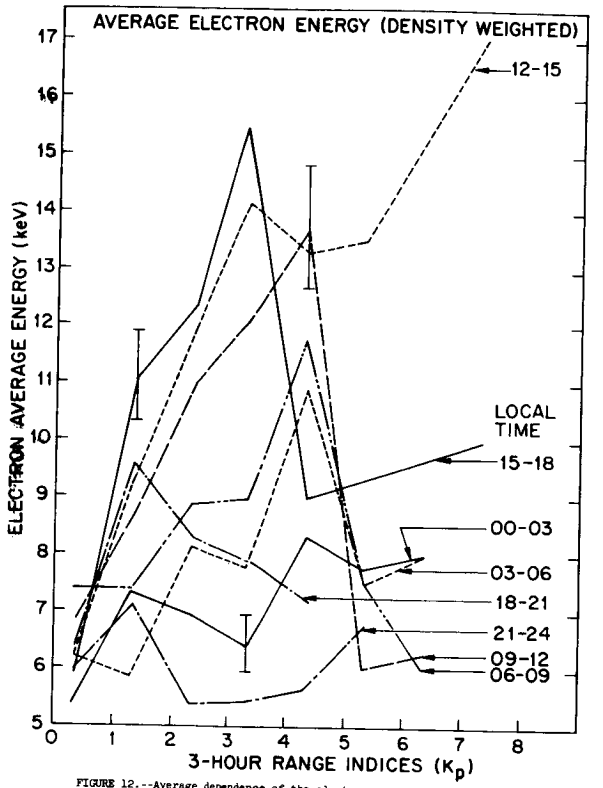

FIGURE 12.--Average dependence of the electron energy on magnetic activity (K_p) for each 3-hour local time segment. The error bars where indicated are one standard deviation on the mean.

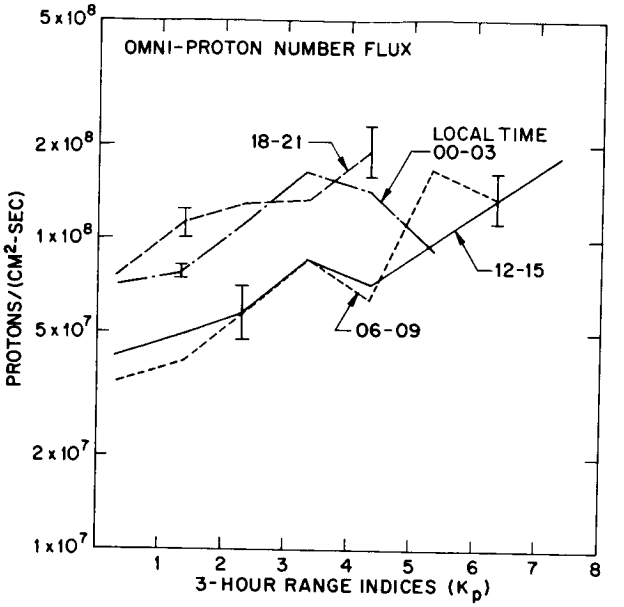

FIGURE 14.--Average dependence of proton flux on magnetic activity (K_p) for four 3-hour local time segments. The behavior of the intermediate time segment was similar. The error bars where shown are the standard deviation on the mean.

Omnidirectional Proton Number Flux (figures 13 and 14): The scatter of the data at all local times is comparable to that shown in figure 13. The relative dependence of the proton flux on K_p does not change rapidly with local time. To avoid unnecessary complications, only every other local time segment curve was included in figure 14. The proton number flux increases smoothly with increased magnetic activity in all local time segments except near local midnight where the flux maximizes around $K_p = 3$. In general the flux increases by about a factor of 2 between $K_p = 0$ and $K_p = 4$.

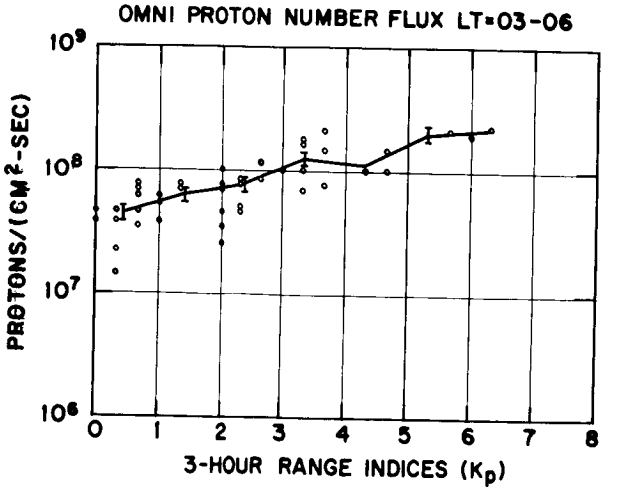

FIGURE 13.--Omnidirectional proton number flux as a function of magnetic activity (K_p) for the local time segment 0300 to 0600. The data points include all samples for this local time segment. The solid line passes through the mean for each ΔK_p interval. The error bars are standard deviations on the mean.

Proton Average Energy (figures 15 and 16): The data scatter in figure 15 is typical for all local time segments. To reduce the confusion, the data in figure 16 is averaged over 6-hour intervals in local time. At low K_p, the average energy is relatively independent of local time. As K_p increases, the average proton energy decreases nearly monotonically for all local times except near local midnight. In the region from 2100 to 0300 LT, the energy decreases with increased magnetic activity up to $K_p \cong 2$, then increases with further increases in magnetic activity. This behavior is nearly reversed from that observed for the proton flux. In general the effect is for the energy flux to remain relatively constant while both the number flux and the average energy change at all local times.

Some of the systematic variation in the plasma parameters with local time and magnetic activity demonstrated in this section can be explained qualitatively on the basis of our present knowledge of the physics of the magnetosphere; however, this is beyond the scope of the present paper. For the physical interpretation of some of the low-energy particle observations in the vicinity of synchronous altitude, see refs. 22-24 and their bibliographies.

SUMMARY

The average low-energy radiation envrionment at synchronous altitude has been shown to vary in a systematic way with respect to local time and magnetic activity. Because of this systematic behavior it may be possible to estimate the low-energy radiation environment for periods of different magnetic activity by utilizing the results of this statistical analysis. The validity of

such estimates can be established only by similar analyses of data for other periods.

Because of the great variability of the low-energy plasma it would be advisable to include particle measurements with future flight experiments on surface damage at synchronous altitude. There are some indications that particle fluxes in the loss cone may exceed the average trapped fluxes by an order of magnitude (ref. 27). This is presently under study at Lockheed by combining simultaneous plasma measurements at synchronous altitude on ATS-5 and at low altitude on OV1-18 near the foot of the field line passing through ATS-5.

ACKNOWLEDGMENTS

The authors would like to thank Drs. R. D. Sharp, R. G. Johnson and M. McCargo for their many helpful suggestions and discussions during this analysis. We would also like to thank L. F. Smith and D. L. Carr for their help in the data reduction and programming. This work was funded by the Lockheed Independent Research Program and by NASA under Contract NAS 5-10392.

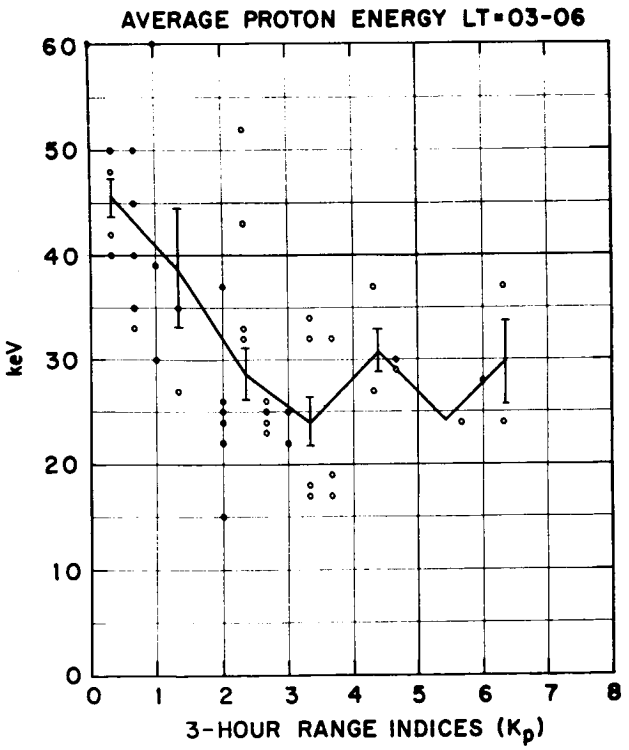

FIGURE 15.--Average proton energy as a function of magnetic activity (K_p) for the local time segment 0300 to 0600. The data points include all one-hour-average samples for this local time segment. The solid line passes through the mean for each ΔK_p interval. The error bars are standard deviations on the mean.

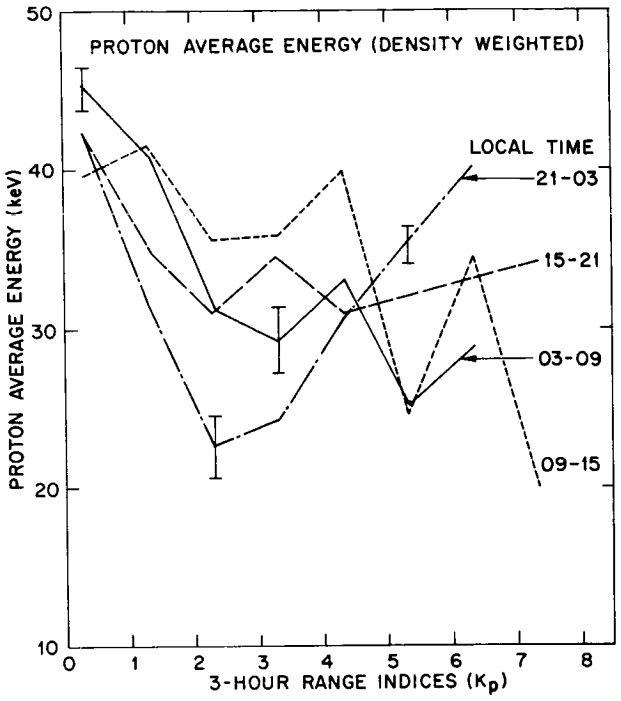

FIGURE 16.--Average dependence of proton average energy on magnetic activity (K_p). The data here were averaged over 6-hour local time segments. The error bars where shown are standard deviations on the mean.

REFERENCES

1. McCARGO, M.; GREENBERG, S.A.; McDONALD, S. L.: Quarterly Progress Report No. 1, NAS 8-26004, July 1970; No. 2, NAS 8-26004, October 1970.
2. McCARGO, M.; GREENBERG, S. A.; and DOUGLAS, N. J.: Prog. in Astronautics & Aeronautics, vol. 23, 1970, p. 189.
3. FOGDALL, L. B.; CANNADAY, S. S.; and BROWN, R. R.: Prog. in Astronautics & Aeronautics, vol. 23, 1970, p. 219.
4. HEANEY, J. B.: Prog. in Astronautics & Aeronautics, vol. 23, 1970, p. 249.
5. McCARGO, M.; GREENBERG, S. A.; and BREUCH, R. A.: NASA Ames Research Center, Final Report, NAS 2-4353, Jan. 1969.
6. GREENBERG, S. A.; MacMILLAN, H. F.; and SKLENSKY, A. F.: NASA/Marshall Space Flight Center, NAS 8-18114, Feb. 1968.
7. BROWN, R. R.; FOGDALL, L. B.; and CANNADAY, S. S.: Prog. in Astronautics & Aeronautics, vol. 21, 1968, p. 697.
8. MILES, J. K.; CHEEVER, P. R.; and ROMANKO, J.: Prog. in Astronautics & Aeronautics, vol. 21, 1968, p. 725.
9. MILLARD, J. P.: Prog. in Astronautics & Aeronautics, vol. 21, 1968, p. 769.
10. SLEMP, W. S.; and HANKINSON, T. W. E.: Prog. in Astronautics & Aeronautics, vol. 21, 1968, p. 797.
11. GREENBERG, S. A.; MacMILLAN, H. F.; and SKLENSKY, A. F.: Air Force Materials Laboratory, AFML-TR-67-294, Sept. 1967.
12. HOLLAND, W. R.: NASA/Ames Research Center, Final Report, NAS 2-3646, Dec. 1967.
13. STREED, E. R.: Prog. in Astronautics & Aeronautics, vol. 20, 1967, p. 237.
14. NEEL, C. B.: Prog. in Astronautics & Aeronautics, vol. 20, 1967, p. 411.
15. SCHAFER, C. F.; and BANNISTER, T. C.: Prog. in Astronautics & Aeronautics, vol. 20, 1967, p. 457.
16. BREUCH, R.A.: Prog. in Astronautics & Aeronautics, vol. 18, 1966, p. 365.
17. JORGENSON, G. V.: Prog. in Astronautics & Aeronautics, vol. 18, 1966, p. 389.
18. MILLER, R. A.; and CAMPBELL, F. J.: Prog. in Astronautics & Aeronautics, vol. 18, 1966, p. 399.
19. GILLETTE, R. G.; BROWN, R. R.; SEILER, R. F.; and SHELDON, W. R.: Prog. in Astronautics and Aeronautics, vol. 18, 1966, p. 413.
20. VETTE, J. I.; LUCERO, A. B.; and KING, J.H.: Vols. III and IV, NASA SP-3024, 1967.
21. HESS, W. N.; MEAD, G. D.; and NAKADA, M. P.: Prog. in Astronautics & Aeronautics, vol. 18, 1966, p. 327.
22. SHARP, R. D.; SHELLEY, E. G.; JOHNSON, R. G.; and PASCHMANN, G.: J. Geophys. Res., vol 75, 1970, p. 6092.
23. SHELLEY, E. G.; SHARP, R. D.; and JOHNSON, R. G.: Radio Science, vol. 6, 1971, in press.
24. DeFOREST, S. E.; and McILWAIN, C. E.: UCSD-SP-70-04, Sept. 1970.
25. REED, R. D.; SHELLEY, E. G.; BAKKE, J. C.; SANDERS, T. C.; and McDANIEL, J. D.: IEEE Trans. Nucl Sci., vol. NS-16, 1969, p. 359.
26. PASCHMANN, G.; SHELLEY, E. G.; CHAPPELL, C. R.; SHARP, R. D.; and SMITH, L. F.: Rev. Sci. Instr., vol. 41, 1970, p. 1706.
27. HONES, E. W., JR.; ASBRIDGE, J. R.; BAME, S. J.; and SINGER, S.: J. Geophys. Res., vol. 73, 1971, p. 63.